Brief Review

Modern Physics Letters A
Vol. 20, No. 15 (2005) 1103–1117

World Scientific
www.worldscientific.com

NEUTRINO MAGNETIC MOMENTS

HENRY T. WONG* and HAU-BIN LI

Institute of Physics, Academia Sinica, Taipei 11529, Taiwan
**htwong@phys.sinica.edu.tw*

Received 25 April 2005

Finite neutrino magnetic moments are consequences of nonzero neutrino masses. The particle physics aspects of the neutrino electromagnetic interactions are reviewed. The astrophysical bounds and the results from recent direct experiments are reviewed, with emphasis on the reactor neutrino experiments. Future projects and prospects are surveyed.

Keywords: Neutrino properties; neutrino interactions; magnetic moments.

PACS Nos.: 14.60.Lm, 13.15.+g, 13.40.Em

1. Introduction

The strong evidence of neutrino oscillations from the solar, atmospheric and long baseline accelerator and reactor neutrino measurements implies finite neutrino masses and mixings.[1,2] Their physical origin and experimental consequences are not fully understood. Experimental studies on the neutrino properties and interactions can shed light to these fundamental questions and provide constraints to the interpretations in the future precision oscillation experiments. New and improved neutrino sources and detector technologies have to be developed in parallel for such studies.

The couplings of neutrinos with the photons are generic consequences of finite neutrino masses, and are one of the important intrinsic neutrino properties[3] to be explored. The neutrino electromagnetic vertex can be parametrized by terms with γ_η and $\sigma_{\eta\xi}$ corresponding to interactions without and with its spin, respectively identified as the "neutrino charge radius" and "neutrino magnetic moments",[4] the latter of which is the subject of this review.

*Corresponding author

2. Particle Physics Overview

The effective Lagrangian for the spin component of the neutrino electromagnetic vertex, depicted schematically in Fig. 1, can be described by

$$L = \frac{1}{2}\bar{\nu}_j \sigma_{\eta\xi}(\beta_{ij} + \varepsilon_{ij}\gamma_5)\nu_i F^{\eta\xi} + \text{h.c.}\,, \tag{1}$$

where $F^{\eta\xi}$ is the electromagnetic field tensor, while ε_{ij} and β_{ij} are respectively the electric and magnetic dipole moments which couple together the neutrino mass eigenstates $(\nu_i)_L$ and $(\nu_j)_R$, resulting in a change of the helicity-states. Cases where $\nu_i = \nu_j$ and $\nu_i \neq \nu_j$ correspond to *diagonal* and *transitional* moments, respectively. Symmetry principles as well as neutrino properties place constraints to the matrices ε_{ij} and β_{ij}.[5] For example, Majorana neutrinos require $\varepsilon_{ii} = \beta_{ii} = 0$ which implies the vanishing of the diagonal moments. The study of neutrino electromagnetic properties is, therefore, in principle a way to distinguish between Dirac and Majorana neutrinos.

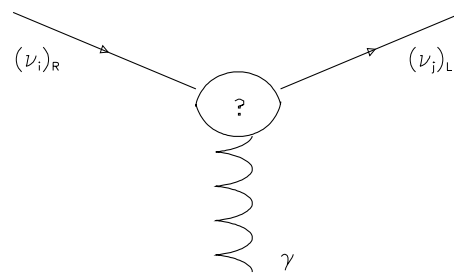

Fig. 1. The schematic diagram of the neutrino–photon interaction vertex which involves a change of the helicity-states.

The experimental observable "neutrino magnetic moment" (μ_ν), usually expressed in units of the Bohr magneton (μ_B), for neutrinos with energy E_ν produced as ν_l at the source and after traversing a distance L can be described by

$$\mu_\nu^2(\nu_l, L, E_\nu) = \sum_j \left| \sum_i U_{li} e^{-iE_\nu L} \mu_{ij} \right|^2 , \tag{2}$$

where $\mu_{ij} \equiv |\beta_{ij} - \varepsilon_{ij}|$ and U_{li} is the neutrino mixing matrix. The observable μ_ν is therefore an effective and convoluted parameter and the interpretations of experimental results depend on the exact ν_l compositions at the detectors. Accordingly, the exact implications of μ_ν limits from reactor experiments, ^{8}B and ^{7}Be solar neutrino experiments are all different.

Given a specific model, μ_ν can be calculated from first principles. Minimally-Extended Standard Model with massive Dirac neutrinos[1] gives $\mu_\nu \sim 10^{-19}[m_\nu/1\text{ eV}]$ which is far too small to have any observable consequences. Incorporation of additional physics, such as Majorana neutrino transition moments

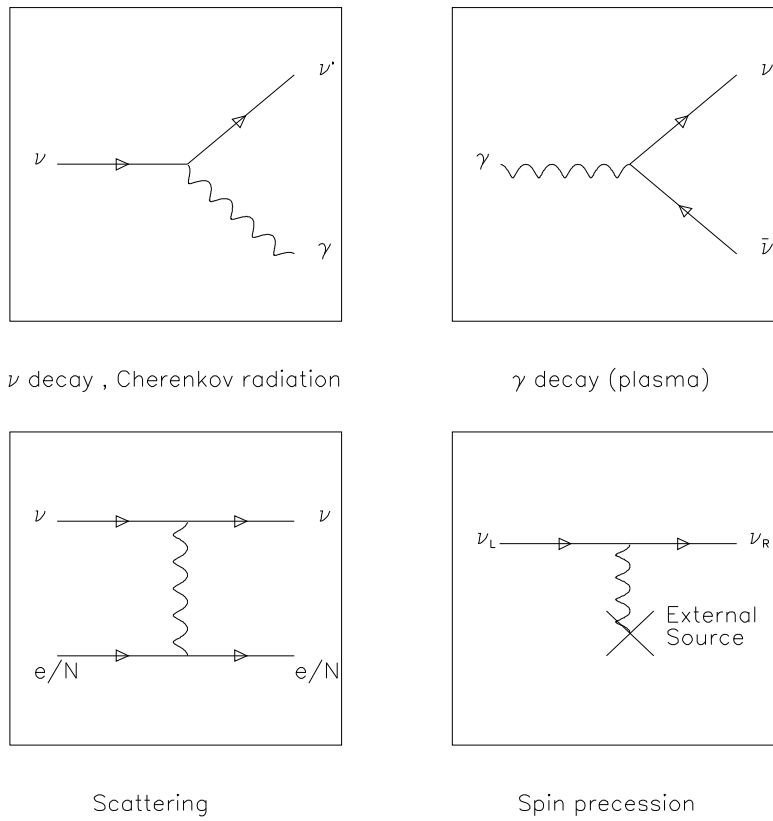

Fig. 2. Schematic diagrams for the various experimental manifestations of neutrino–photon couplings.

or right-handed weak currents, can significantly enhance μ_ν to the experimentally relevant ranges.[1,6] Supersymmetry as well as extra dimensions[7] can also contribute to the process.

Information on μ_ν can be derived from astrophysics arguments as well as from direct laboratory experiments. A finite neutrino magnetic moment can be manifested in many processes,[8] as shown schematically in Fig. 2. In particular, studies of neutrino–electron scatterings are the most sensitive, robust and established methods. The cross-section can be written as a sum of the Standard Model (SM) and the magnetic moment (μ_ν) processes[6]:

$$\frac{d\sigma}{dT}(\nu + e \to \nu + e) = \left(\frac{d\sigma}{dT}\right)_{\mathrm{SM}} + \left(\frac{d\sigma}{dT}\right)_{\mu_\nu} . \tag{3}$$

The Standard Model contribution is

$$\left(\frac{d\sigma}{dT}\right)_{\mathrm{SM}} = \frac{G_{\mathrm{F}}^2 m_e}{2\pi}\left[(g_V + g_A)^2 + (g_V - g_A)^2\left(1 - \frac{T}{E_\nu}\right)^2 + (g_A^2 - g_V^2)\frac{m_e T}{E_\nu^2}\right], \tag{4}$$

where m_e is the electron mass, E_ν is the incident neutrino energy, T is the experimentally observable electron recoil energy, and the couplings are given by

$$g_V = \begin{cases} 2\sin^2\theta_W + \dfrac{1}{2} & \text{for } \nu_e\,, \\ 2\sin^2\theta_W - \dfrac{1}{2} & \text{for } \nu_\mu, \nu_\tau\,, \end{cases}$$
$$g_A = \begin{cases} \dfrac{1}{2} & \text{for } \nu_e\,, \\ -\dfrac{1}{2} & \text{for } \nu_\mu, \nu_\tau \end{cases} \tag{5}$$

while the substitution $g_A \to -g_A$ should be made for anti-neutrinos $(\bar{\nu}_e, \bar{\nu}_\mu, \bar{\nu}_\tau)$. To incorporate the charge radius (denoted by $\langle r^2\rangle$) contributions which do not change the helicity-states, the substitution $g_V \to g_V + x$ can be used, where $x = \frac{2}{3}M_W^2\langle r^2\rangle \sin^2\theta_W$.

A finite neutrino–photon coupling manifested as magnetic moment μ_ν would give rise to an additional contribution in the ν-e scattering differential cross-section

$$\left(\frac{d\sigma}{dT}\right)_{\mu_\nu} = \frac{\pi\alpha_{em}^2}{m_e^2}\left[\frac{1 - T/E_\nu}{T}\right]\mu_\nu^2\,. \tag{6}$$

Since a change of the neutrino helicity-states is involved contrary to that in SM interactions, there is no interference between the two processes.

The neutrino radiative decay for the process $\nu_i \to \nu_j + \gamma$ is another manifestation of the neutrino electromagnetic couplings which results in the emission of a final-state real photon. Gauge invariance dictates that the helicities between the initial and final states neutrino must be different. The decay rate Γ_{ij} is related to μ_{ij} via[9]

$$\Gamma_{ij} = \frac{1}{8\pi}\frac{(m_i^2 - m_j^2)^3}{m_i^3}\mu_{ij}^2\,, \tag{7}$$

where $m_{i,j}$ are the masses for neutrino mass-eigenstates $\nu_{i,j}$.

3. Astrophysics Bounds

Astrophysics bounds on μ_ν were mostly derived from the consequences from a change of the neutrino helicity-states in the astrophysical medium.[1,8] These include studies in the available degrees of freedom in Big Bang Nucleosynthesis, stellar cooling via plasmon decay, and the cooling of supernova 1987a. The typical range is $\mu_\nu(\text{astro}) < 10^{-10}$–$10^{-12}\ \mu_\text{B}$.

The bounds, however, depends on modeling of the astrophysical systems and on placing certain assumptions on the neutrino properties. The supernovae cooling arguments only apply for Dirac neutrinos where the right-handed state is sterile and can leave the astrophysical objects readily. Another generic assumption is the

absence of other nonstandard neutrino interactions except for the anomalous magnetic moments. For more realistic studies, a global treatment would be desirable, incorporating oscillation effects, matter effects as well as the complications due to interference and competitions among various channels.

The spin-flavor precession (SFP) mechanism, with or without matter resonance effects in the solar medium, has been used to explain solar neutrino deficit.[10] The solar ν_e would interact with solar magnetic field $B_\odot$ via its magnetic moment to become $\nu_x (x \neq e)$. This scenario is in fact compatible with all solar neutrino data. The terrestrial KamLAND experiment, however, recently confirmed the Large Mixing Angle (LMA) parameter space of the matter oscillation scenario as *the* solution for the solar neutrino problem,[11] such that SFP can be excluded as the dominant contribution in solar neutrino physics. Conversely, coupling the LMA allowed region with the recent KamLAND solar-$\bar{\nu}_e$ bounds[12] of $\bar{\nu}_e/\nu_\odot < 2.8 \times 10^{-4}$, a constraint on $\int \mu_\nu [B_{\odot\perp}] dr$ can be derived for Majorana neutrinos, where $B_{\odot\perp}$ is the transverse component of the solar magnetic field. Recent work[13] on the modeling of $B_\odot$ turned this into bounds on the magnetic moments, also in the range of $\mu_\nu(^8\text{B-}\nu_\odot) < 10^{-10}$–$10^{-12}$ μ_B.

4. Recent Results from Direct Experiments

Direct laboratory experiments on neutrino magnetic moments utilize solar, accelerator and reactor neutrinos as sources, and are conducted under controlled conditions. These approaches are robust and avoid the ambiguities and model-dependence in the astrophysical bounds. The experiments require an understanding of the neutrino energy spectra and compositions at the detectors by independent means. They typically study neutrino–electron scatterings $\nu_l + e \to \nu_x + e$. The signature is an excess of events over those due to Standard Model (SM) and other background processes, which exhibit the characteristic $1/T$ spectral dependence. Limits from negative searches are valid for both Dirac and Majorana neutrinos and for both diagonal and transitional moments. However, interpretations and comparisons among various experiments should take into account the difference in the flavor compositions between them *at* the detectors.

4.1. *Solar neutrinos*

Data from the solar neutrino and KamLAND experiments firmly established the validity of the Standard Solar Model (SSM) predictions of the solar neutrino flux, as well as the LMA-matter oscillation solution being the leading mechanism of neutrino flavor conversion in the Sun. This can be used as the basis of magnetic moment searches with solar neutrino data.

The Super-Kamiokande (SK) Collaboration performed spectral distortion analysis of their electron recoil spectral due to ^{8}B solar neutrino–electron scattering.[14] The study was to look for $1/T$ excess over an oscillation "background" at the 5–14 MeV energy range. SK data alone allowed a large region of (Δm^2, $\tan^2\theta$)

parameter space and could only set limit of $\mu_\nu(^8\text{B-}\nu_\odot) < 3.6 \times 10^{-10}\ \mu_\text{B}$ at 90% Confidence Level (CL). Coupling with constraints from the other solar neutrino and KamLAND results, the LMA region is uniquely selected as *the* solution, such that a more stringent limit of $\mu_\nu(^8\text{B-}\nu_{\odot;\text{LMA}}) < 1.1 \times 10^{-10}\ \mu_\text{B}$ at 90% CL was derived.

The Borexino Collaboration performed analysis of their Counting Test Facility data at the ^{7}Be solar neutrino relevant range: 200–500 keV.[15] Subtracting the known $^{14}\text{C}\beta$-spectrum and *assuming* an additional linear background, a fit to look for a $1/T$ spectrum did not indicate any excess and a limit of $\mu_\nu(^7\text{Be-}\nu_\odot) < 5.5 \times 10^{-10}\ \mu_\text{B}$ at 90% CL was derived, using SSM ^{7}Be $\nu_\odot$ flux.

An innovative insight is that neutrino magnetic moments can induce photo-dissociation in deuterium. The agreement between SNO neutral-current measurements with SSM $\nu_\odot$-flux predictions placed constraints of $\mu_\nu(^8\text{B-}\nu_\odot) < 3.7 \times 10^{-9}\ \mu_\text{B}$ at 95% CL.[16]

4.2. *Accelerator neutrinos*

Accelerators provide neutrinos with known flavor compositions. The timing structures can be used for background subtraction. Compared to reactor neutrinos, the lower flux as well as higher energy limit the sensitivities. However, neutrinos of all three flavors are produced at accelerators such that this is the only laboratory avenue for studying magnetic moments from ν_μ and ν_τ.

The LSND experiment measured "single electron" events from a beam with known ν_e, ν_μ and $\bar{\nu}_\mu$ fluxes and spectral compositions.[17] Taking the SM calculated values of $\sigma(\nu_\mu\text{-}e)$ and $\sigma(\bar{\nu}_\mu\text{-}e)$ which were confirmed by other experiments, the derived value of $\sigma(\nu_e\text{-}e)$ agreed well with SM predictions and provided a measurement of $\sin^2\theta_W = 0.248 \pm 0.051$. Limits of $\mu_\nu(\nu_e) < 1.1 \times 10^{-9}\ \mu_\text{B}$ and $\mu_\nu(\nu_\mu) < 6.8 \times 10^{-10}\ \mu_\text{B}$ at 90% CL were derived from the absence of excess of counts.

The DONUT experiment first observed explicit ν_τ charged-current interactions[18] showing the ν_τ flux at a beam dump configuration is consistent with the expected level. The experiment also looked for "single-electron" events at cross-sections much larger than SM expectations. One event was observed while the predicted background from other known sources was 2.3.[19] This was converted into a magnetic moment limit for ν_τ: $\mu_\nu(\nu_\tau) < 3.9 \times 10^{-7}\ \mu_\text{B}$ at 90% CL.

4.3. *Reactor neutrinos*

Reactor neutrino experiments provide the most sensitive laboratory searches for the magnetic moments of $\bar{\nu}_e$, taking advantages of the high $\bar{\nu}_e$ flux, low E_ν and better experimental control via the reactor ON/OFF comparison. Experimental signatures for μ_ν would be an excess of events between the reactor ON over OFF samples, which exhibits an $1/T$ energy dependence.

The $\bar{\nu}_e$'s emitted in power reactors are produced through β-decays of (a) the fission products, following the fission of the four dominant fissile isotopes: ^{235}U,

Table 1. Neutrino yields and the relative contributions from the dominant $\bar{\nu}_e$ sources in typical power reactors.

Channels	$\bar{\nu}_e$-yield/event	Relative rate/fission
^{235}U fission	6.14	~ 0.49
^{238}U fission	7.08	~ 0.07
^{239}Pu fission	5.58	~ 0.36
^{241}Pu fission	6.42	~ 0.08
$^{238}\mathrm{U}(n,\gamma)^{239}\mathrm{U}$	2.0	0.6

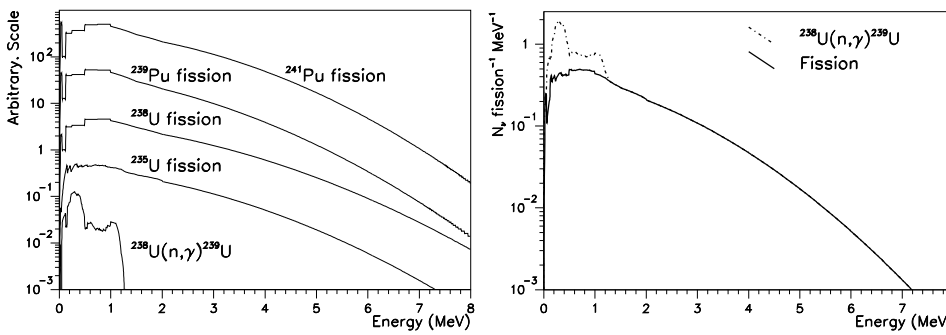

(a) (b)

Fig. 3. (a) Spectral shape for reactor neutrinos due to individual production channels. (b) Total spectra at typical power reactor operation.

^{238}U, ^{239}Pu and ^{241}Pu, and (b) ^{239}U, following the neutron capture on the ^{238}U fuel [$^{238}\mathrm{U}(n,\gamma)^{239}\mathrm{U}$]. The $\bar{\nu}_e$-yield for these channels, as well as their relative contributions per fission are summarized in Table 1, while their individual $\bar{\nu}_e$ spectra are depicted in Fig. 3(a). The typical total reactor $\bar{\nu}_e$ spectra[6,20] ($\phi(\bar{\nu}_e)$) are depicted in Fig. 3(b). The fluxes are about 6 $\bar{\nu}_e$ per fission extending to about 8 MeV, and 1.2 $\bar{\nu}_e$ per fission with an endpoint at 1.3 MeV[21] for the fission and neutron capture $\bar{\nu}_e$'s, respectively.

The measured differential spectrum from the Bugey-3 experiment[22] showed that $\phi(\bar{\nu}_e)$ can be evaluated to a few % accuracy at $E_\nu > 3$ MeV using the standard reactor operation data as input. However, many beta-decay channels and other additional effects have to be considered[20] for the evaluation of $\phi(\bar{\nu}_e)$ below 3 MeV. These had neither been measured experimentally nor thoroughly addressed theoretically, and therefore $\phi(\bar{\nu}_e)$ is subjected to much bigger uncertainties at this low energy range, affecting the focuses and strategies of magnetic moment searches with reactor neutrinos.

The differential cross-sections of the relevant neutrino interactions due to typical reactor neutrino spectra are shown in Fig. 4. It can be seen that magnetic moment effects at the range of 10^{-10} μ_B from $\bar{\nu}_e$-e scatterings, as described by Eq. (6),

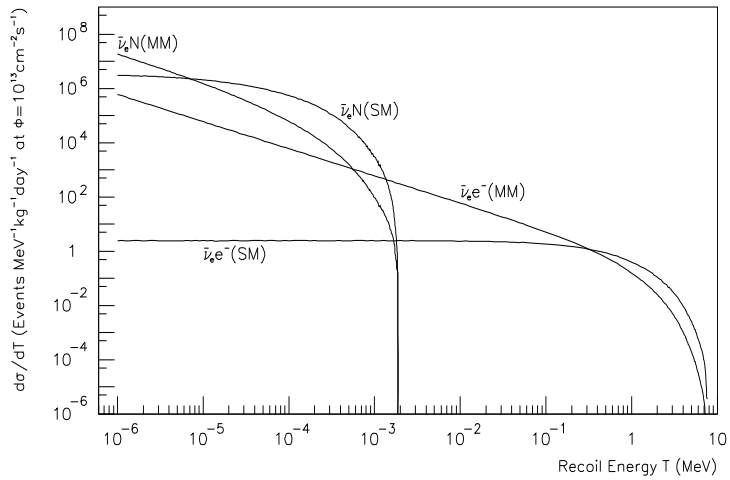

Fig. 4. Differential cross-section showing the recoil energy spectrum in $\bar{\nu}_e$-e and coherent $\bar{\nu}_e$-N scatterings, at a reactor neutrino flux of 10^{13} cm^{-2}s^{-1}, for the Standard Model (SM) processes and due to a neutrino magnetic moment (MM) of 10^{-10} $\mu_{\rm B}$.

dominate over the other processes within the range from 1 keV to 1 MeV. The dominant contribution below 1 keV is from the Standard Model neutrino–nucleus ($\bar{\nu}_e$-N) coherent scatterings, as described by:

$$\left(\frac{d\sigma}{dT}\right)^{\rm coh}_{\rm SM} = \frac{G_{\rm F}^2}{4\pi} m_N [Z(1-4\sin^2\theta_W) - N]^2 \left(1 - \frac{m_N T_N}{2E_\nu^2}\right), \tag{8}$$

where m_N, N and Z are the mass, neutron number and atomic number of the nuclei, respectively, and T_N is the measureable recoil energy of the nucleus. At very low (below 10 eV) recoil energies, the $\bar{\nu}_e$-N coherent scatterings due to magnetic moment effects at 10^{-10} $\mu_{\rm B}$ become dominant, as described by:

$$\left(\frac{d\sigma}{dT}\right)^{\rm coh}_{\mu_\nu} = \frac{\pi\alpha^2\mu_\nu^2}{m_e^2} Z^2 \left(\frac{1 - T_N/E_\nu}{T_N} + \frac{T_N}{4E_\nu^2}\right) \tag{9}$$

in the case for scatterings on spin-zero nuclei.

Neutrino–electron scatterings were first observed in the pioneering experiment[23] at Savannah River where plastic scintillators were adopted as target surrounded by NaI(Tl) crystal scintillators as anti-coincidence counters. A revised analysis of the data[6] with improved input on the reactor neutrino spectra as well as the electroweak parameters indicated an excess of events over SM expectations which could be interpreted as a positive signature for a finite μ_ν at $\mu_\nu(\bar{\nu}_e) \sim 2$–$4 \times 10^{-10}$ $\mu_{\rm B}$. An intrinsic error source of this experiment was the use of a proton-rich target. The cross-section for the $\bar{\nu}_e + p \to e^+ + n$ reaction is much larger than that for $\bar{\nu}_e$-e scatterings. This neutrino-induced channel could not be suppressed by the standard reactor ON/OFF subtraction, and may become an important background contribution.

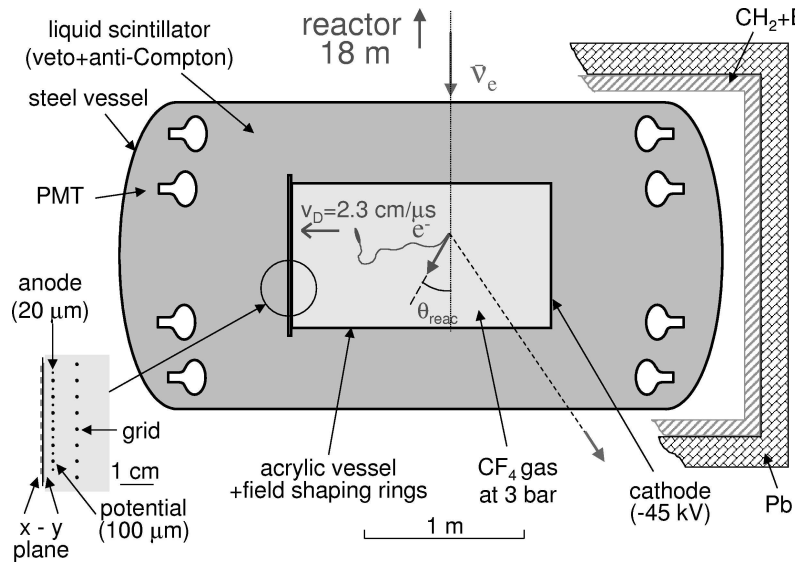

Fig. 5. Schematic layout of the the MUNU experiment, adopting Time Projection Chamber tracking approach.

Subsequent $\bar{\nu}_e$-e scattering experiments with reactor neutrinos all adopted proton-free design in the choice of target and ambient materials. Other results came from the Kurtchatov[24] and Rovno[25] experiments which quoted limits of $\mu_\nu(\bar{\nu}_e) < 2.4 \times 10^{-10}\ \mu_\mathrm{B}$ and $\mu_\nu(\bar{\nu}_e) < 1.9 \times 10^{-10}\ \mu_\mathrm{B}$ at 90% CL, respectively. However, many experimental details, in particular the effects due to the uncertainties in the SM background, were not discussed.

The MUNU experiment[26] at the Bugey reactor in France deployed a Time Projection Chamber (TPC) filled with 11.4 kg of CF_4 gas at 3 bar, surrounded by active liquid scintillator as anti-Compton vetos, as displayed schematically in Fig. 5. It gave excellent single-electron event selection and measured the scattering angle with respect to the reactor core direction. Neutrino events are scattered "forward" such that a forward/background comparison was used to extract the possible neutrino events, where "background" were events scattered towards the backward, upward and downward cone.

The residual "forward-background" spectrum from 66.6 days of reactor ON data at a threshold of 700 keV is shown in Fig. 6(a). The excess rate of $1.07 \pm 0.34\ \mathrm{day}^{-1}$ is consistent with the Standard Model prediction, though the $\chi^2/\mathrm{dof} = 11.5/7$ (goodness-of-fit $p \sim 10\%$) is only marginal and may indicate residual systematic effects. In particular, the lowest-energy bin shows a $\sim 2\sigma$ excess over the SM values. The magnetic moment thus derived was $\mu_\nu(\bar{\nu}_e) < 0.9 \times 10^{-10}\ \mu_\mathrm{B}$ at 90% CL.

The residual spectrum of a 1 bar low-pressure run with 5.3 days of reactor ON data is displayed in Fig. 6(b). While the statistical errors and the uncertainties in the reactor spectra evaluation[20] are too large for quantitative conclusions to be

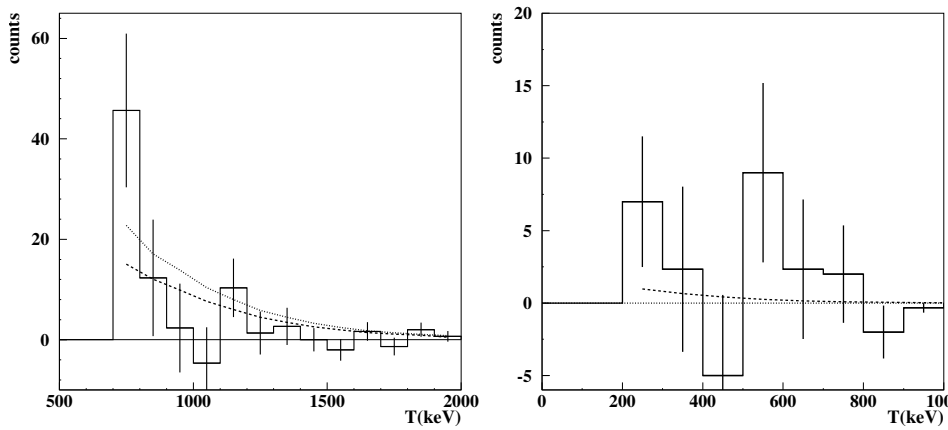

(a) (b)

Fig. 6. Reactor-ON forward-background residual spectra from the MUNU experiment with (a) 66.6 days of data at 3 bar pressure and 700 keV threshold (b) 5.3 days of data at 1 bar pressure and 200 keV threshold. Dashed lines show Standard Model predictions while dotted line is the 90% CL limit for magnetic moment searches.

drawn, the data demonstrated that a gas TPC can be used to measure energies and directions down to the ~ 100 keV range, opening up a possible avenue for the real-time measurement of the low-energy pp solar neutrinos.

The TEXONO Collaboration adopted a compact all-solid design with a high-purity germanium detector (HPGe) 1.06 kg in mass, surrounded by anti-Compton detectors of NaI(Tl) and CsI(Tl) scintillators, as depicted in Fig. 7. The assembly was further covered by a radon purge system, passive shieldings and plastic scintillators veto panels. The shieldings were constructed with 50 tons of materials including, from inside out, OFHC copper, boron-loaded polyethylene, stainless steel and lead. The measurement was performed at the Kuo-Sheng (KS) Power Plant in Taiwan.

The focus was on the $T = 10$–100 keV range for the enhanced signal rates and robustness in the control of systematic uncertainties. At this energy range, the $\bar{\nu}_e$-e scattering rates due to magnetic moments are much larger than the SM rates at the 10^{-10} $\mu_{\rm B}$ sensitivity level being explored (by a factor of 20 at $T = 10$ keV), so that uncertainties in the irreducible SM background can be neglected.[20] In addition, $T \ll E_\nu$ such that the μ_ν-related scattering rates depend on the *total* neutrino flux (ϕ_ν) rather than the poorly-known details of the low-energy reactor neutrino spectra. The total neutrino flux is well known and can be evaluated accurately from reactor operation data — every fission is expected to produce about 6 and 1.2 $\bar{\nu}_e$'s due to β-decays of the fission daughters and of ^{239}U following neutron capture on ^{238}U, respectively.

Comparing 4712/1250 hours of reactor ON/OFF data, no excess of events was found and with an analysis threshold of 12 keV just above the complications due

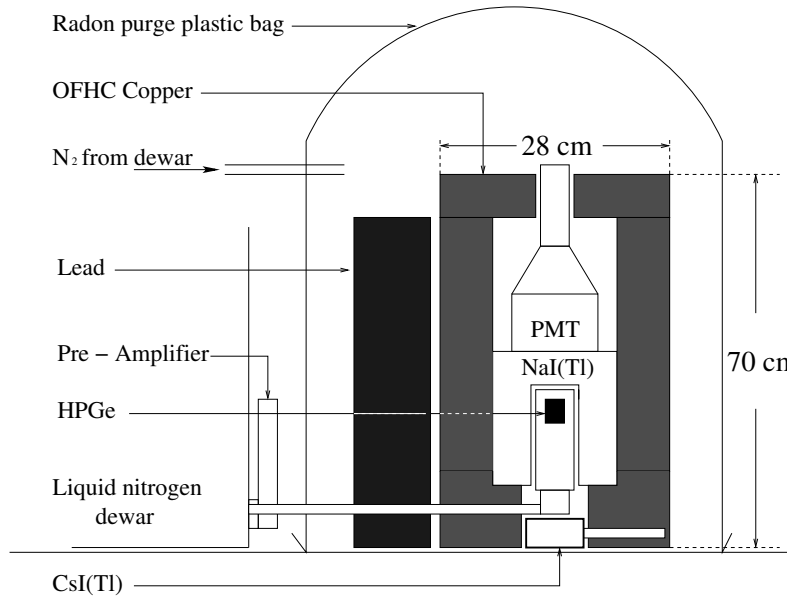

Fig. 7. The TEXONO-KS experiment, deploying high-purity germanium detector for low threshold.

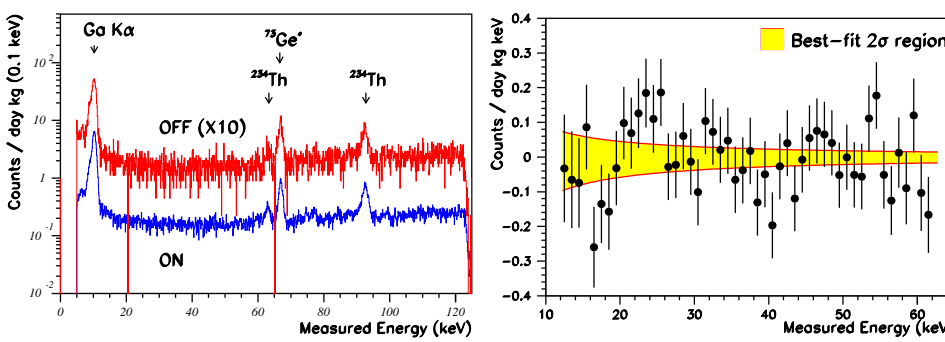

(a) (b)

Fig. 8. Energy spectra from the TEXONO-KS experiment, for (a) 4712/1250 hours of reactor ON/OFF data, and (b) the ON−OFF residual.

to atomic effects, a limit of $\mu_\nu(\bar{\nu}_e) < 1.3 \times 10^{-10}\ \mu_B$ at 90% CL was derived from a best-fit with $\chi^2/\text{dof} = 48/49$ (goodness-of-fit $p \sim 50\%$). The ON/OFF and residual spectra are displayed in Fig. 8. In addition, a background level of $\sim 1\ \text{kg}^{-1}\text{keV}^{-1}\text{day}^{-1}$ at the 10–20 keV range was achieved — a comparable range to those from the underground Dark Matter experiments.

Depicted in Fig. 9(a) is the summary of the results in $\mu_\nu(\bar{\nu}_e)$ searches versus the achieved threshold in reactor experiments. The dotted lines denote the

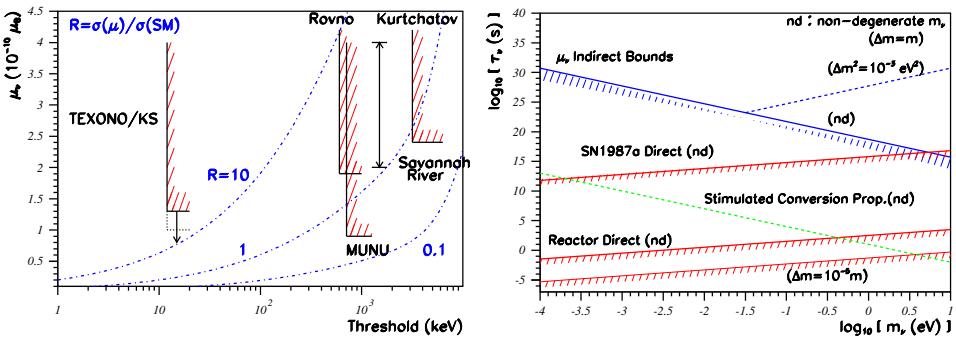

(a) (b)

Fig. 9. Summary of the results in (a) the searches of neutrino magnetic moments with reactor neutrinos, and (b) the bounds of neutrino radiative decay lifetime.

$R = \sigma(\mu)/\sigma(SM)$ ratio at a particular $[T, \mu_\nu(\bar{\nu}_e)]$. The large R-values for the KS experiment imply that its results are robust against the uncertainties in the SM cross-sections. In particular, the limits remain valid in the case where there are not-yet-accounted-for sources of neutrinos. Indirect bounds on the neutrino radiative decay lifetimes can be inferred from Eq. (7) and displayed in Fig. 9(b) for the scenario where a single channel dominates the transition. It corresponds to $\tau_\nu m_\nu^3(\bar{\nu}_e) > 1.2 \times 10^{19}$ eV^{3}s at 90% CL in the non-degenerate case. It can be seen that ν-e scatterings give much more stringent bounds than the direct searches.[27]

The KS low threshold data also allowed an analysis of reactor electron–neutrino (ν_e) to be performed.[28] Realistic neutron-transport simulations indicated that the leading contributions of ν_e-emissions at a reactor are from the neutron capture on ^{50}Cr and ^{54}Fe in the stainless steel at the control rod assembly and in the reactor core construction materials. The process produces ^{51}Cr and ^{55}Fe which subsequently decay via electron capture with the emissions of mono-energetic ν_e's at 747 keV and 231 keV, respectively, giving a total yield of about 8.3×10^{-4} ν_e per fission. Using similar selection and analysis procedures devised for $\bar{\nu}_e$'s, direct limits on the ν_e magnetic moment and the radiative lifetime of $\mu_\nu(\nu_e) < 1.3 \times 10^{-8}$ μ_B and $\tau_\nu/m_\nu(\nu_e) > 0.11$ s/eV at 90% CL, respectively, were derived, from the absence of excess events between reactor ON/OFF data. Indirect bound of $\tau_\nu m_\nu^3(\nu_e) > 5.7 \times 10^{14}$ eV^{3}s at 90% CL was also inferred from the magnetic moment results using Eq. (7). While the sensitivities are not competitive to those from reactor $\bar{\nu}_e$, the studies provide direct probes on the ν_e properties without assuming CPT invariance, and cover possible anomalous matter effects which may differentiate ν_e from $\bar{\nu}_e$.

4.4. *Global analysis*

A global analysis was performed[29] fitting simultaneously the magnetic moment data from the reactor and solar neutrino experiments, and the LMA oscillation

parameters constrained by solar neutrino and KamLAND results. Only Majorana neutrinos were considered such that there were only transition moments. A "total" magnetic moment vector $\Lambda = (\mu_{23}, \mu_{31}, \mu_{12})$ was defined, such that its amplitude was given by $|\Lambda|^2 = \frac{1}{2}\,\mathrm{Tr}(\mu^+\mu)$. A global fit produced 90% CL limits of $|\Lambda| < 4.0 \times 10^{-10}\ \mu_\mathrm{B}$ from solar and KamLAND data, and $|\Lambda| < 1.8 \times 10^{-10}\ \mu_\mathrm{B}$ when reactor data were added. The results indicate the role of reactor experiments in constraining the magnetic moment effects.

5. Future Projects and Prospects

The sensitivities for neutrino magnetic moments in direct search experiments scale as

$$\mu_\nu \propto \frac{1}{\sqrt{N_\nu}} \left(\frac{B}{Mt}\right)^{1/4}, \tag{10}$$

where N_ν is the signal events at some reference magnetic moments, B, M, t are the background level, detector mass and measurement time, respectively. The best strategy to enhance the sensitivities is to increase on N_ν, which is proportional to the neutrino flux ϕ_ν and is related to the detection threshold in recoil energy T.

The atomic energy level effects[30] limit the potential sensitivity improvement by reducing T only. For example, N_ν only increases by a factor of three with a lowering of detection threshold from 10 keV to 10 eV in germanium. Therefore, big statistical boost in μ_ν will most favorably be achieved by an increase in ϕ_ν — while keeping the systematics in control via (a) lowering the detection threshold to retain the "$\mu_\nu \gg$ SM" event-rate requirements, and (b) maintaining a low background level. Since the minimal energy transfer to the atomic electrons would be ~ 100 eV, it follows from condition (a) that such an approach of enhancing ϕ_ν and reducing T may only be applicable for $\mu_\nu \to 10^{-13}\ \mu_\mathrm{B}$.

The GEMMA experiment[31] under preparation at the Kalininskaya Nuclear Reactor in Russia is similar to the TEXONO-KS approach, aiming at an improvement to $\mu_\nu(\bar{\nu}_e) \to 3 \times 10^{-11}\ \mu_\mathrm{B}$ by locating at a closer distance, using a larger mass target and operating at a lower threshold. The MAMMONT project,[32] currently at the R&D phase, has ambitious specifications of deploying a 40 MCi (4 kg) tritium source with a flux of $6 \times 10^{14}\ \mathrm{cm^{-2}s^{-1}}$ on ultra-sensitive detectors with threshold down to 10 eV, either with cryogenic silicon detectors or germanium with internal amplification. The projected sensitivity is $\mu_\nu(\bar{\nu}_e) \to 2.5 \times 10^{-12}\ \mu_\mathrm{B}$.

The TEXONO Collaboration continued data taking with the HPGe at KS. Sensitivities to the $7 \times 10^{-11}\ \mu_\mathrm{B}$ range can be expected. In parallel, a CsI(Tl) crystal scintillator array[33] with a total mass of 200 kg is collecting data. The focus is on the high (> 3 MeV) recoil energy range to perform a first measurement of SM neutrino–electron scattering at the MeV momentum transfer range. A 5-g "ultra-low-energy" germanium prototype is being tested, where the goal is to develop into a 1-kg Ge-array detector for the first experimental observation of neutrino–nucleus coherent scattering and WIMP dark matter searches. As by-product, such

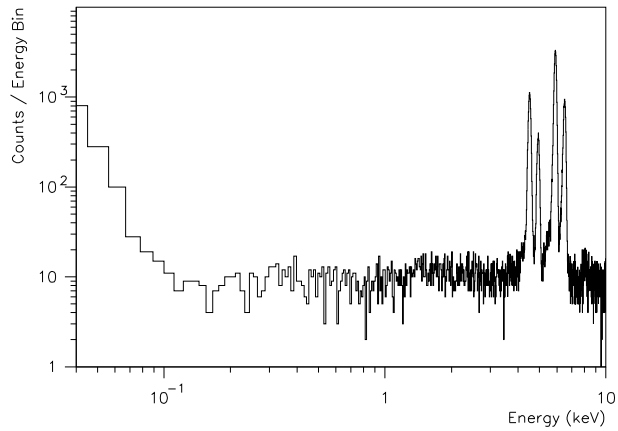

Fig. 10. Energy spectrum with the ultra-low energy germanium detector prototype indicating a detector threshold lower than 100 eV, The peaks are from an ^{55}Fe source and from back-scattering with Ti.

an experiment will potentially probe $\mu_\nu(\bar{\nu}_e) \to 2 \times 10^{-11}\ \mu_{\rm B}$. An energy threshold of 100 eV has been achieved[34] with the prototype, as illustrated in Fig. 10, while background studies at the sub-keV range are under way, both at the KS Lab as well as in the Yang–Yang underground laboratory in South Korea.

Alternatives of neutrino sources such as artificial radioactive sources[35] and accelerator-based β-sources[36] have been discussed, using NaI(Tl), liquid scintillator and large TPC as detectors. The projected sensitivity range is $\mu_\nu \sim \text{few} \times 10^{-11}\ \mu_{\rm B}$.

6. Outlook

The magnetic moments of the neutrino parametrize its coupling with the photons and are sensitive to its masses and mixings, as well as its Dirac or Majorana nature. It is, therefore, a *conceptually* rich subject with much neutrino physics and astrophysics to be explored. However, there are no indications of any measurable/observable signals in the current and future rounds of experimental efforts. Improvement in sensitivities will necessarily involve new neutrino sources as well as novel neutrino detection techniques and channels. These advances may find important potential applications in other areas of neutrino and underground physics experimentations.

References

1. See the respective sections in *Review of Particle Physics*, Particle Data Group, *Phys. Lett.* **B592** (2004) for details and references.
2. For latest status, see, for example, *Proc. of XXI Conf. on Neutrino Phys. & Astrophys.*, ed. J. Dumarchez, *Nucl. Phys. B* (*Proc. Suppl.*) **143** (2005) and references therein.
3. A. de Gouvea, *Nucl. Phys. B* (*Proc. Suppl.*) **143**, 167 (2005).

4. H. T. Wong, *Nucl. Phys. B* (*Proc. Suppl.*) **143**, 205 (2005).
5. B. Kayser, *Phys. Rev.* **D26**, 1662 (1982); J. F. Nieves, *ibid.* **D26**, 3152 (1982).
6. P. Vogel and J. Engel, *Phys. Rev.* **D39**, 3378 (1989), and references therein.
7. R. N. Mohapatra, S. P. Ng and H. B. Yu, *Phys. Rev.* **D70**, 057301 (2004).
8. G. G. Raffelt, *Stars as Laboratories for Fundamental Physics* (Univ. Chicago Press, 1996).
9. G. G. Raffelt, *Phys. Rev.* **D39**, 2066 (1989).
10. J. Barranco *et al.*, *Phys. Rev.* **D66**, 093009 (2002), and references therein.
11. T. Araki *et al.*, *Phys. Rev. Lett.* **94**, 081801 (2005).
12. K. Eguchi *et al.*, *Phys. Rev. Lett.* **92**, 071301 (2004).
13. E. Kh. Akhmedov and J. Pulido, **553**, 7 (2003); O. G. Miranda *et al.*, *Phys. Rev. Lett.* **93**, 051304 (2004).
14. D.W. Liu *et al.*, *Phys. Rev. Lett.* **93**, 021802 (2004).
15. H. O. Back *et al.*, *Phys. Lett.* **B563**, 35 (2003).
16. J. A. Grifols, E. Masso and S. Mohanty, *Phys. Lett.* **B587**, 184 (2004).
17. L. B. Auerbach *et al.*, *Phys. Rev.* **D63**, 112001 (2001).
18. K. Kodama *et al.*, *Phys. Lett.* **B504**, 218 (2001).
19. R. Schwienhorst *et al.*, *Phys. Lett.* **B513**, 23 (2001).
20. H. B. Li and H. T. Wong, *J. Phys.* **G28**, 1453 (2002), and references therein.
21. V. I. Kopeikin, L. A. Mikaelyan and V. V. Sinev, *Phys. Atom. Nucl.* **60**, 172 (1997).
22. B. Achkar *et al.*, *Phys. Lett.* **B374**, 243 (1996).
23. F. Reines, H. S. Gurr and H. W. Sobel, *Phys. Rev. Lett.* **37**, 315 (1976).
24. G. S. Vidyakin *et al.*, *JETP Lett.* **55**, 206 (1992).
25. A. I. Derbin *et al.*, *JETP Lett.* **57**, 769 (1993).
26. Z. Daraktchieva *et al.*, hep-ex/0502037, and references therein.
27. H. B. Li *et al.*, *Phys. Rev. Lett.* **90**, 131802 (2003), and references therein.
28. B. Xin *et al.*, hep-ex/0502001.
29. W. Grimus *et al.*, *Nucl. Phys.* **B648**, 376 (2003); M. A. Tortola, hep-ph/0401135.
30. V. I. Kopeikin *et al.*, *Phys. Atom. Nucl.* **60**, 2032 (1997).
31. A. G. Beda *et al.*, *Phys. Atom. Nucl.* **61**, 66 (1998).
32. L. N. Bogdanova, *Nucl. Phys.* **A721**, 499 (2003).
33. H. T. Wong *et al.*, *Astropart. Phys.* **14**, 141 (2000); Y. Liu *et al.*, *Nucl. Instrum. Meth.* **A482**, 125 (2002).
34. H. T. Wong, *Mod. Phys. Lett.* **A19**, 1207 (2004).
35. I. R. Barabanov *et al.*, *Astropart. Phys.* **8**, 67 (1997); A. Ianni and D. Montanino, *ibid.* **10**, 331 (1999).
36. G. C. McLaughlin and C. Volpe, *Phys. Lett.* **B591**, 229 (2004); C. Volpe, *Nucl. Phys. B* (*Proc. Suppl.*) **143**, 43 (2005).